The droplet race: Optimization of a wettability gradient surface

Graham Danny Koyeerath, Yann Favennec, Bruno Auvity, Christophe Josset

▶ **To cite this version:**

Graham Danny Koyeerath, Yann Favennec, Bruno Auvity, Christophe Josset. The droplet race: Optimization of a wettability gradient surface. Physics of Fluids, 2024, 36 (3), 10.1063/5.0191507 . hal-04523557

HAL Id: hal-04523557
https://hal.science/hal-04523557

Submitted on 28 Mar 2024

HAL is a multi-disciplinary open access archive for the deposit and dissemination of scientific research documents, whether they are published or not. The documents may come from teaching and research institutions in France or abroad, or from public or private research centers.

L'archive ouverte pluridisciplinaire **HAL**, est destinée au dépôt et à la diffusion de documents scientifiques de niveau recherche, publiés ou non, émanant des établissements d'enseignement et de recherche français ou étrangers, des laboratoires publics ou privés.

The droplet race: optimization of a wettability gradient surface

Graham Danny Koyeerath, Yann Favennec, Bruno Auvity, and Christophe Josset*
Laboratory of Thermal and Energy Nantes, Nantes Université, Nantes– 44300, France

(*Electronic mail: christophe.josset@univ-nantes.fr)

(Dated: March 28, 2024)

Droplet behavior influenced by wettability distribution is a pertinent field of research with applications in lab-on-a-chip and heat transfer devices amongst others. Some have proposed patterned surfaces with controlled variation of wettability to orient the direction of the droplet motion or to increase its velocity. This patterns are arrived upon with experience and knowledge of this phenomenon. In this research paper, authors take a mathematical approach to the physical problem by using a gradient based optimizer for maximizing droplet velocity. Given some initial conditions, the optimizer marches towards the optimum wettability distribution profile. The droplet motion is modeled in two dimensions (2D) (i.e. on the xy-plane), on a plate having a wettability distribution in one dimension (1D) (i.e. along x-axis). The single component pseudopotential model (SCMP) allows for the quantification of the wettability distribution as a distribution of a pseudo-density of the solid nodes of the flat plate. Starting with several monotonous analytical profiles, quadratic convex profile allows to reach the maximum mean velocity for the threshold droplet displacement. Different sets of initial profiles, length of the plate (L) and diameter of the droplet (D) are tested. For smaller L/D ratio, the optimal wettability distributions exhibit non trivial features: profiles can be non monotonous, and wettability gradient could be locally null. With the increase of L/D ratio, these specificities tend to be less prominent and optimal profiles converge to the quadratic convex one. The main innovation and significance of the paper is that mathematical optimization algorithms have been used conjointly with a multiphase LBM solver to address for the first time the droplet race defined as: "what is the best wettability profile in order for a droplet to reach a desired location as quickly as possible ?"
Keywords: droplet motion, multiscale optimization, multiphase optimization, pseudopotential model, LBM, brachistochrone problem.

I. INTRODUCTION

In nature, droplet movement on a still surface occurs mainly due to air currents or gravity (in case of an inclined surface). Recently, unexpected directional motion (without external energy supply) of a liquid droplet on the Araucaria leaf[1] was reported and later this phenomenon has been reproduced numerically[2]. Meanwhile, in a controlled environment, the droplet motion is possible due to either active or passive methods of generating a wettability gradient[3]. Surfaces employed specifically for this purpose are in literature called as wettability gradient surfaces (WGS). Active methods include temperature gradients[4] (first documented in the seminal work of Marangoni[5]), mechanical vibrations[6], electrostatic potential, etc., while passive techniques require surface chemical treatments or alteration of surface topography[7,8]. A realistic surface is non-ideal as surface roughness due to topographical imperfections is commonplace. Also a bare surface gathers dirt or residue being exposed to chemical reactions (including corrosion) or deposits due to phenomenon such as evaporation over a period of time. This degrades the performance of WGS with the passage of time as the droplet motion could be inhibited due to pinning defects.

WGS have multiple applications where droplet transport is required. These surfaces could be used for orienting the direction of a moving droplet[9]. It could also function as pump in micro-scale devices. One major application for a WGS is the lab-on-a-chip (LOC) device which handles fluids even at submicroscopic scale[10]. LOCs have further applications in nano technology, bio-engineering, sensors, etc. Liquid transport plays an important role in heat transfer process especially during phase change[11]. In condensation processes, hybrid wettability surfaces improved performances allowing droplet condensation on hydrophobic places whereas droplets are drained toward hydrophilic places and removed due to gravity[12,13]; the use of a WGS could then prevent the formation of a liquid film. Also these surfaces could be useful for self-cleaning, where the droplet picks up dirt as it is propelled forward; few inclined hydrophobic surfaces have already been used for this purpose[14,15].

This phenomenon of a wettability gradient initially theoretically studied[16,17] has been experimentally verified for chemical surface treatments and thermal gradients on an inclined plate[18]. Various theoretical explanations have been put forward providing for different analytical formulations for droplet velocity[19,20] assuming steady state motion. Numerical simulations have on the other hand been used to investigate situations which are difficult to recreate in an experimental setup. Spatial and temporal fluctuations[21] of the wettability, wettability gradients induced by chemical reactions[22], various wettability distribution profiles[23] and droplet spreading[24] on patterned surfaces, to mention a few studies, have all been explored via numerical modeling to promote/influence droplet motion.

The numerical simulations for a droplet on a surface could be divided into two categories: in the former category the contact angle is prescribed and the fluid behavior (pressure, velocity, etc.) for different configurations are obtained a posteriori. In the latter category the interaction forces are prescribed and both the contact angle and fluid behavior are obtained after numerical solving. While the former category includes macroscopic models, most often coupling Navier-Stokes equations with an interface tracking methods, like Volume of fluid (VOF)[3] or level set (LS), the latter category includes molecular dynamics and mesoscopic methods like Van der Waal model[25]

or the lattice Boltzmann model (LBM)[26]. Multiphase LBM generally exhibits a diffused interface being devoid of the interface tracking equations. In the case of the pseudopotential method[26], this interface and the contact angle are directly a result of the interparticle forces. These forces are present both between each fluid particles and between fluid and solid particles. Among all the multiphase LBM models (color gradient, phase field, free energy and pseudopotential), the pseudopotential method is used the most commonly[27] and it is known for its efficiency and simplicity as it generally does not employ the Poisson equation for pressure. These factors play a significant role in the authors selection of this method for the optimizer, as it requires multiple reruns of the physical simulation (hereafter also referred to as the forward problem).

So, even if the motion of a droplet submitted to a wettability gradient is a well documented phenomenon, both experimentally and numerically, the question of the optimization of this displacement remains untreated. Indeed, from the performed bibliography survey, it appears that wettability gradient has always been assumed to be constant, i.e. the wettability distribution is restricted to the linear profile, and the main result is, the steeper the gradient, the greater the mean velocity[16,28]. Now the wettability cannot vary indefinitely, i.e. this property is bounded, from superhydrophobicity to superhydrophilicity. Consequently, the steeper the gradient, the shorter the displacement length of the droplet. The significance of the study lies in resolving the conflict between the spread of a bounded property (wettability) and the displacement length to achieve highest mean velocity. In other words, for a droplet to seamlessly travel the desired length, the question of the optimal wettability profile seems to have no trivial solutions, and, to the best knowledge of the authors, this has not been addressed yet. Note that, in the field of optimization applied on multiphase flow, an adjoint-state gradient-based shape optimizer demonstrated its competency of propelling a droplet with a variation of surface tension, such an optimizer being based on an approximated two-phase Stokes equations with no solid-fluid interaction[29,30]. Another shape optimizer has been employed on the surface topography in order to control the droplet shape, without motion[31].

The implication of the current study is that increasing the mean velocity of droplets using specific WGS would improve, for example, the flow rate of LOC device or the performances of condensers. From an optimization and historical point of view, this problem loosely resembles the brachistochrone problem. The objective of the brachistochrone problem was to find the optimal geometrical path which would be covered by a sliding bead starting from rest at a given location (with gravity and without friction) in order to reach the final location in the shortest time interval[32]. The analytical approaches proposed by five different mathematicians found that a cycloid, rather than a simple constant step is the best shape for the task. So, for a given gravitational potential, i.e. a starting height and a final height, optimization analytical process identified an optimal structure profile. An innovation of this article is the manner of approaching the problem, i.e. similar to the brachistochrone problem, one searches for the best shape or profile of wettability distribution for a WGS. The only difference is that a numerical optimization algorithm is used here rather than an analytical approach (if at all one exists).

In the context of the article the forward problem consists of a droplet resting on a horizontal surface which is a WGS. No pinning effect (i.e. no contact angle hysteresis) on the interface between the droplet and the solid is assumed (i.e. the surface is assumed ideal for the simulation). The optimization process is for finding the optimum wettability distribution profile so that the droplets moves as quickly as possible to a desired location. The simulation is performed in two dimensions of space while the wettability evolves in one dimension. Although three-dimensional (3D) effects are not taken into account in this paper, such a geometric assumption seems not to affect the mean velocity of the droplet, referring to 2D/3D literature comparison[3], whereas it allows for substantial computational benefits.

Section II describes the methodology of optimization. In this section, we discuss the cost function of the optimization problem, we then elaborate on the forward problem model, we build the parameterization of the control variable, and set-up the optimizer. Section III gives the performance of several wettability distributions defined by some simple analytical function, and section IV gives some results of optimization. Ultimately, section V presents the conclusions of this research paper.

II. OPTIMIZATION PROBLEM SET-UP

A. Cost function definition

The objective of the study is to maximize the droplet velocity on a flat plate by adjusting the distribution of wettability. The mean velocity is computed when the droplet reaches a certain desired location ($\widetilde{C}_{\text{drop}}$). Here locations and droplet positions are indicated in terms of the droplet center of gravity (denoted as C_{drop}). The droplet center of gravity is computed as:

$$C_{\text{drop}}(t) = \frac{\int_{\mathcal{D}_\text{f}} (\rho(\boldsymbol{r},t) - \rho_{\text{vap}}) r_x \, \mathrm{d}\boldsymbol{r}}{\int_{\mathcal{D}_\text{f}} (\rho(\boldsymbol{r},t) - \rho_{\text{vap}}) \, \mathrm{d}\boldsymbol{r}}, \tag{1}$$

where, r_x is the x-component of location vector i.e. $\boldsymbol{r}$ for a 2D domain such that the droplet moves along the x-axis on the xy-plane, ρ is the density at $\boldsymbol{r}$ and at time t, ρ_{vap} is the density of the vapor and $\mathcal{D}_\text{f}$ is the fluid domain restriction.

Mathematically, maximization of the mean velocity consists in maximizing the following cost function:

$$\mathcal{J} = \frac{C_{\text{drop}}|_{t=t_f} - C_{\text{drop}}|_{t=0}}{t_f}, \tag{2}$$

where the final time t_f is the time given a posteriori when $|C_{\text{drop}} - \widetilde{C}_{\text{drop}}|$ reaches a very small user-defined value.

B. Lattice Boltzmann method

The forward model on which the optimizer relies is based on the Lattice Boltzmann Method (LBM). For a detailed discus-

sion on LBM, the reader may refer to[27,33]. Briefly, LBM is a numerical solver of the classical Boltzmann transport equation of probability distribution functions f. Under some assumptions, one can recover the Navier-Stokes equations, modeling the fluid flow at macroscale, using LBM representing the fluid behavior at the mesoscale.

The Boltzmann equation is discretized in space, $\boldsymbol{r}$, in time, t, and along velocity directions, $\boldsymbol{e}_i$. From the knowledge of probability distribution functions f_i, macroscopic quantities like density, ρ, and velocity, $\boldsymbol{u}$, for example, are retrieved:

$$\rho = \sum_i f_i; \quad \rho \boldsymbol{u} = \sum_i \boldsymbol{e}_i f_i. \tag{3}$$

Note that this density is the one to be used in the computation of the droplet center of gravity eq. (1) used in the cost function definition eq. (2). As far as this paper is concerned, physical simulations are performed using the single component pseudopotential model[34] (This model was initially described by Shan and Chen[35]). The explicit solver for the i^{th} velocity direction is described as:

$$f_i(\boldsymbol{r} + \Delta\boldsymbol{r}, t + \Delta t) - f_i(\boldsymbol{r}, t) = \Lambda_i + \mathscr{F}_{i,\text{edm}}. \tag{4}$$

In eq. (4), the collision operator Λ is approximated by a relaxation time model. The multiple relaxation time (MRT) model[36,37] and by extension the MRT collision operator (Λ_{mrt}), has been chosen in view of both its stability and accuracy. Eventually, the last operator involved in this equation, $\mathscr{F}_{\text{edm}}$, represents the exact difference forcing (EDM) scheme used for incorporating action of external forces[38].

In the context of this paper, external forces, $\boldsymbol{F}_{\text{T}}$, acting on a node located within the fluid domain, η, are constituted of three distinct forces: the fluid-fluid inter-particular force $\boldsymbol{F}_{\text{p}}$ (1st term in the RHS of eq. (5)), the solid-fluid inter-particular force $\boldsymbol{F}_{\text{s}}$ (2nd term in the RHS of eq. (5)), and the gravitational body force $\boldsymbol{F}_{\text{body}}$ (third term in the RHS of eq. (5)):

$$\begin{aligned} \boldsymbol{F}_{\text{T}} \;=\; & -G\psi(\eta) \sum_{\substack{i \\ \vartheta_i = \eta + \Delta t \boldsymbol{e}_i \in \mathcal{D}_{\text{f}} \\ |\vartheta_i - \eta| \le \sqrt{2}}} w_{\text{fr},i}\psi(\vartheta_i)\boldsymbol{e}_i \\ & -G\psi(\eta) \sum_{\substack{i \\ \vartheta_i = \eta + \Delta t \boldsymbol{e}_i \in \mathcal{D}_{\text{s}} \\ |\vartheta_i - \eta| \le \sqrt{2}}} w_{\text{fr},i}\psi(\vartheta_i)\boldsymbol{e}_i \\ & +\rho g_{\text{grav}}. \end{aligned} \tag{5}$$

In eq. (5), w_{fr} is the forcing weight function, G is the interaction strength, ϑ_i is the neighboring node in the i^{th} direction, $\mathcal{D}_s$ represents (the nodes in) the solid domain, g_{grav} is the gravitational constant and the space-dependent function ψ is the so-called pseudopotential function. The pseudopotential, which is a function of the density, is related to the real pressure p of the fluid:

$$\psi = \sqrt{\frac{2(p - \rho e_s^2)}{G e_s^2}}. \tag{6}$$

where, e_s is the speed of sound in the LBM paradigm.

This fluid pressure can be resolved using different realistic equations of state[39]; the Carnahan-Starling (CS) equation of state was used to model the diphasic fluid model:

$$p_{\text{cs}} = \rho RT \frac{1 + b\rho/4 + (b\rho/4)^2 - (b\rho/4)^3}{(1 - b\rho/4)^3} - a\rho^2 \tag{7}$$

in which $a = 0.4963R^2T_c^2/p_c$ and $b = 0.18727RT_c/p_c$ are constants. Here, R is universal gas constant in LBM units, T is the temperature and T_c is the critical temperature, while p_c is the corresponding critical pressure in the LBM paradigm. It was demonstrated[40] that for a particular value of b the diffused interface thickness can be controlled by the value of a.

The formulation of the solid-fluid inter-particular force $\boldsymbol{F}_{\text{s}}$ enables the quantification of wettability in terms of the fictitious density of (adjacent) solid nodes. This density, denoted as ρ_{w}, is referred to as pseudo-density[33]. Varying the pseudo-density from ρ_{liq} to ρ_{vap}, a contact angle between 0° and 180° can be obtained. This mapping allows for a correlation between the static contact angle θ_{stat} and the pseudo-density. Figure 1 depicts the correlation between θ_{stat} and the normalized pseudo-density $\left(\rho_{\text{w}}^* = (\rho_{\text{w}} - \rho_{\text{vap}})/(\rho_{\text{liq}} - \rho_{\text{vap}})\right)$. This correlation is consistent across different temperatures T (which is specified relative to the critical point temperature T_c). The static contact angle is unknown a priori and is obtained after the simulation of a droplet resting on a flat horizontal plate with constant wettability. This approach is different from macroscopic methods where contact angle is directly prescribed. As such, LBM is apt for such optimization studies.

The variation of the pseudo-density (wettability) along the length of the plate causes droplet motion which is successfully captured by LBM due to its transient nature. Figure 1 illustrates the droplet motion, where $\mathscr{I}_{\text{lbm}}$ is the iteration number i.e. time in the LBM paradigm. Also the fluid streamlines are shaded according to the fluid velocity. The droplet motion occurs for a linear wettability distribution (denoted hereafter as Υ_{lin}), and no pinning effects. Small vortices can be observed in the vicinity of the droplet interface; these are the spurious currents. As the droplet travels forward, a continuous flux of vapor can be observed along with the formation of its boundary layer on the top and the bottom of the flat plate. This vapor flux is an artifact caused by the use of periodic boundary conditions. Both these artifacts have negligible impact on the droplet velocity and shape, hence these are ignored. The forward problem validation is detailed in appendix B.

C. Parameterization of control variables

The space-dependent pseudo-density is the control variable which is tweaked to maximize the mean velocity of the droplet. Its physical interpretation was given above in section II B. This pseudo-density being continuous, a discrete counterpart version is used for the optimization algorithm. As far as this paper is concerned, the discretization is performed using the n linear Lagrange basis functions $\mathscr{L}_m(r_x)$. This originates from the optimization domain having n nodes uniformly spaced one from the other (so using $q = n - 1$ elements, all of equal

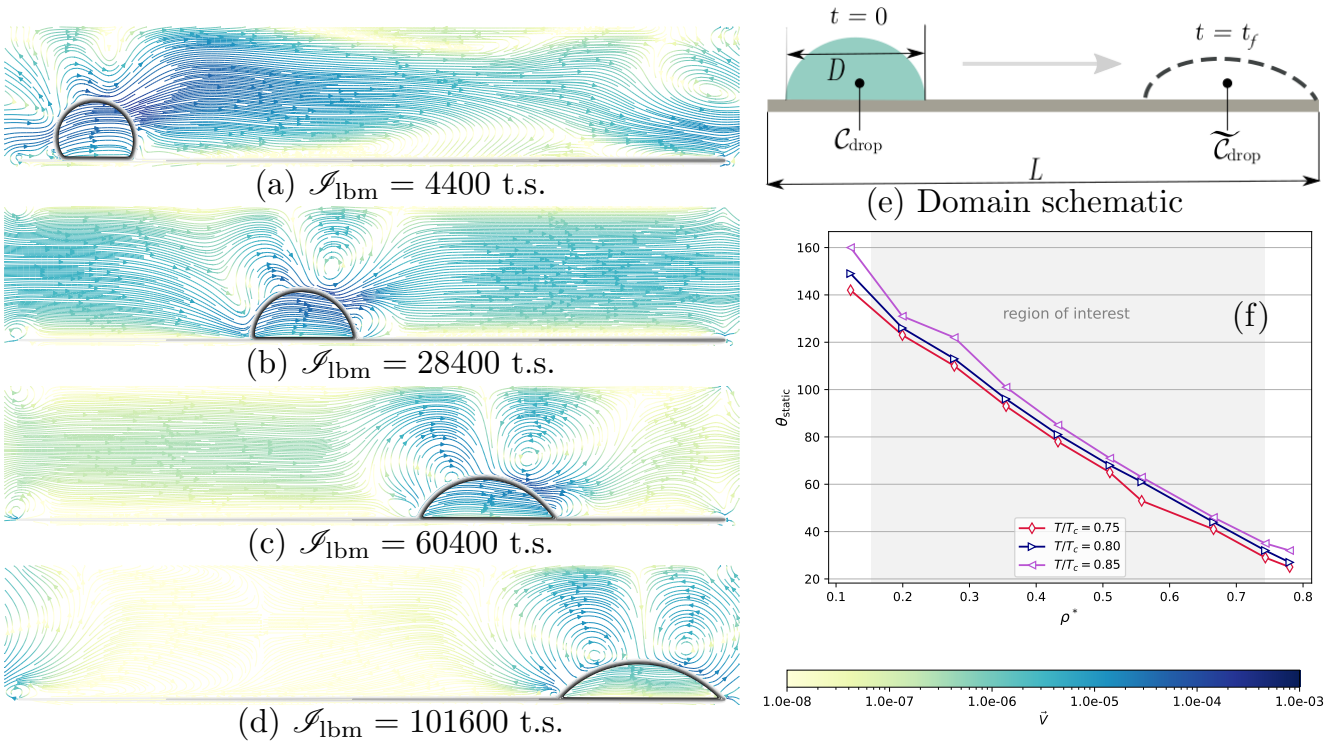

Figure 1: (a-d) LBM simulation for droplet motion on a linear wettability profile flat plate at $T/T_c = 0.75$; (e) illustrates the domain schematics; (f) Correlation between static contact angle (θ_{stat}) and pseudo-density of the solid plate

length). The relationship between the continuous control variable, $\rho_{\mathrm{w}}(r_x)$, and the discrete one, $\boldsymbol{\rho}_{\mathrm{w}}$ is:

$$\boldsymbol{\rho}_{\mathrm{w},\boldsymbol{m}} = \rho_{\mathrm{w}}(r_{x_m}); \quad \rho_{\mathrm{w}}(r_x) = \sum_{m=1}^{n} \mathscr{L}_m(r_x)\boldsymbol{\rho}_{\mathrm{w},\boldsymbol{m}}. \tag{8}$$

D. Optimizer

Gradient based steepest descent optimizer[41] is used for arriving at an optimum solution. For a given parameterization, the update step is given as:

$$\boldsymbol{\rho}_{\mathrm{w}}^{(k+1)} = \boldsymbol{\rho}_{\mathrm{w}}^{(k)} - \xi^{(k)}\, \nabla\mathcal{J}(\boldsymbol{\rho}_{\mathrm{w}}^{(k)}). \tag{9}$$

In eq. (9), superscripts denote the iteration count, $\nabla\mathcal{J}$ is the cost function gradient (i.e. it gathers partial derivatives of the cost function with respect to each parameter $\boldsymbol{\rho}_{\mathrm{w},\boldsymbol{m}}$, where $m = 1, \ldots, n$); the finite difference method is used to compute the cost function gradient. Eventually, ξ is a positive scalar value that minimizes $\mathcal{J}(\boldsymbol{\rho}_{\mathrm{w}}^{(k+1)})$; a dichotomy strategy is used to do so.

From experience it becomes apparent that, performing the optimization with a small number of elements ($q \leq 8$) in the parameterization process inhibits attaining a WGS with high droplet velocities due to lack of resolution of the control variable. On the contrary, beginning the optimization process with a large number of elements ($q \geq 128$) leads the optimizer to quickly reach local minima only, but far away from the global one. Thus we follow the multiscale parameterization described in[42]. The optimization process consists in maximizing the cost function eq. (2) for a small number of elements q using the update eq. (9), until stabilization of the control variable, then double the number of elements, and repeat the whole process until global stabilization is reached. Algorithm 1 describes schematically this multiscale optimization algorithm. Note that the control variables is allowed to fluctuate within the predetermined limits (further explanation in section II E).

Algorithm 1: General flow of a multiscale optimization algorithm

Input: Pseudo-density state $\boldsymbol{\rho}_{\mathrm{w}}^{(0)} \in \mathcal{D}_{\mathrm{s}}$
Initialize $\boldsymbol{f}$, ρ and $\boldsymbol{u}$ for the fluid domain ($\mathcal{D}_{\mathrm{f}}$).
Choose appropriate initial optimization element number: $q^{(0)}$
while ($q^{(z)} \leq q_{\max}$) **do**
  while ($\|\boldsymbol{\rho}_w^{(k)} - \boldsymbol{\rho}_w^{(k+1)}\|_1 \geq \gamma_{\mathrm{c}}$; *where* γ_{c} *is a constant.*) **do**
    Compute the Boltzmann variables $\boldsymbol{f}$ solving eq. (4)
    Compute the cost function $\mathcal{J}$ i.e. eq. (2)
    Compute the gradient ($\nabla\mathcal{J}$) using finite difference
    Compute the gradient step size (ξ) using dichotomy line search algorithm
    Update the pseudo-density using eq. (9)
  Update element number: $q^{(z+1)} = 2q^{(z)}$
return *Optimum wettability distribution* $\boldsymbol{\rho}_w^{(\dagger)}$

E. Forward problem setup

The range of the non-dimensional pseudo-density is limited such that $\rho_w^* \in [0.152, 0.742]$. Thus superhydrophobic and superhydrophilic regions are avoided. The artificial limit is placed to ensure stability of simulation where density ratio is high ($\rho_{liq}/\rho_{vap} > 10$). Table I describes the geometric parameters like the plate sizes along with the corresponding domain sizes and also the value of the constraints, i.e. $\widetilde{C}_{drop}$. These parameters have been chosen in order to ensure stability of simulations. Table II details liquid and vapor densities as well as surface tension, all of these physical properties being obtained for the CS EOS at different temperatures, see eq. (7). Periodic boundary conditions are used to ensure domain inter-connectivity. For a temperature value of $T/T_c = 0.75$ the corresponding density ratio is $\rho_{liq}/\rho_{vap} \approx 30$. The Bond number (Bo = $g_{grav} D^2 \Delta\rho/(4\sigma)$, where D is the droplet diameter) of the simulations lies in the range given as Bo $\in [0.001424, 0.02279]$. The corresponding range of mean capillary number ($Ca_{avg} = \nu_{liq}\rho_{liq}\mathcal{J}/\sigma$, where $\mathcal{J}$ is the cost function, i.e. the mean droplet velocity) for simulations lies in the range such that $Ca_{avg} \in [0.0236, 0.0456]$. In the lattice Boltzmann paradigm as the simulation occurs in the mesoscopic scale, the unit system used differs from the real world. Hence the correlation between the two different systems is usually expressed in terms of the relevant non-dimensional numbers.

Many factors influence the motion of the droplet on a surface. The current study proposes a novel manner of attaining the optimum wettability distribution. As such this article lacks an analysis on the complete list of parameters. In the current context, the influence of the size of the droplet (relative to surface area/size) on the optimization results is looked into. In the following sections, results of different simulations are discussed.

Table I: Domain size, plate length and objective used for simulations.

	Plate length (l.u.)	Domain size	$\widetilde{C}_{drop}$ (l.u.)
small plate	256	277×101	189
medium plate	512	533×101	417
large plate	1024	1045×201	844

Table II: Fluid densities and surface tension(σ) at different temperatures for the LBM model (simulation results)

	ρ_{liq}	ρ_{vap}	σ
$T/T_c = 0.75$	0.333	0.011	0.0090417
$T/T_c = 0.80$	0.306	0.0193	0.0063263
$T/T_c = 0.85$	0.2777	0.03	0.0040333

III. PRIOR TO OPTIMIZATION

Three groups of simulations were performed for this research paper. The first group of simulations are only forward LBM simulations, without any optimization algorithm coupled to them. This study, which precedes the optimization studies in section IV, and which is the context of this preliminary results section, is done to ascertain values for the optimization constraints, and narrow down the region of search for our optimization study.

Five different wettability profiles corresponding to curves which are monotonous in nature are tested on the medium sized plate, see fig. 2a. The equations of these curves can been obtained from the appendix A. The objectives here are twofold: to find a good initial wettability profile for a suitable starting point, and also to find appropriate values for constraints $\widetilde{C}_{drop}$ and $\mathcal{I}_{lbm}^{max}$ (this latter is a maximum time constraint in the forward LBM simulation). Figure 2b provides us with the evolution of the droplet center of gravity as the simulation proceeds. It is apparent that the relative performance of each profile Υ is dependent on $C^*_{drop} = C_{drop}/L$. Below in eq. (10), the order of performance (in terms of cost function value) is mentioned at three points in the simulation:

$$\text{if} \quad C^*_{drop} = \begin{cases} 0.3 \text{ then } \mathcal{J}(\Upsilon_{cca}) > \mathcal{J}(\Upsilon_{qca}) > \mathcal{J}(\Upsilon_{lin}) > \mathcal{J}(\Upsilon_{qcv}) > \mathcal{J}(\Upsilon_{ccv}). \\ 0.4 \text{ then } \mathcal{J}(\Upsilon_{qca}) > \mathcal{J}(\Upsilon_{cca}) > \mathcal{J}(\Upsilon_{lin}) > \mathcal{J}(\Upsilon_{qcv}) > \mathcal{J}(\Upsilon_{ccv}). \\ 0.6 \text{ then } \mathcal{J}(\Upsilon_{lin}) > \mathcal{J}(\Upsilon_{qca}) > \mathcal{J}(\Upsilon_{qcv}) > \mathcal{J}(\Upsilon_{cca}) > \mathcal{J}(\Upsilon_{ccv}). \end{cases} \tag{10}$$

Moreover, the final center of gravity ($C_{drop}|_{t=t_f}$) for each droplet is different though the leading edge of all the droplets arrive at the end of the plate. This difference can be explained by the difference in the droplet curvature which in turn is due to the spatial wettability distribution under the belly of the droplet. Now, considering the final center of gravity of the droplet for each individual wettability profile, with no time constraint, i.e. $C^*_{drop} = C^*_{drop}\big|_{t=t_f}$, then the order of performance is:

$$\mathcal{J}(\Upsilon_{qcv}) > \mathcal{J}(\Upsilon_{lin}) > \mathcal{J}(\Upsilon_{qca}) > \mathcal{J}(\Upsilon_{ccv}) > \mathcal{J}(\Upsilon_{cca}). \tag{11}$$

This means that, for this given objective, the highest mean droplet velocity is for the quadratic convex wettability profile Υ_{qcv}. It appears that even with very simple wettability profiles, the definition of the best one is sensitive to the ob-

jective function definition. So, further in the article (for the optimization process) , $\widetilde{\mathcal{C}}_{\text{drop}}$ is chosen such that this objective can be reached with the constant gradient wettability profile Υ_{lin}. The value of the constraint for each plate sizes is given in table I. The maximum iteration number $\mathcal{J}_{\text{lbm}}^{\max}$ is fixed in a similar manner. The linear (Υ_{lin}) and the quadratic convex (Υ_{qcv}) profiles, will be used hereafter as initial guesses.

IV. RESULTS AND DISCUSSION

Three sets of optimization simulations are performed to understand how the optimizer behaves in different situations. To begin with, section IV A presents an optimization test based on the multiscale approach in which the parameterization is progressively refined. As the resolution increases, the route taken by the optimizer to the optimal WGS is examined. Next, section IV B discusses the study on the dependency of the obtained solutions on the initial wettability profile. Lastly, in section IV C, different plate length to droplet diameter L/D ratio are used for testing the sensitivity of the optimized profiles with respect to both these parameters. Section IV D then presents the applicability of obtained optimal wettability profiles.

A. Progressive refinement of the parameterization

For the small plate ($L/D = 3.2$), the route embarked on by the multiscale optimization algorithm is illustrated in fig. 3. The successive wettability profiles are obtained after attaining convergence for each respective optimization scale. The initial linear wettability profile, Υ_{lin}, is firstly updated after performing optimization at the first scale, on the 2-elements parameterization, to obtain Υ_{10}. Considering the proximity of Υ_{10} and Υ_{qcv}, relative to Υ_{lin}, it can be said that the optimizer approaches in the direction of Υ_{qcv}. Now, optimization at the next scale (with the 4-elements parameterization) gives Υ_{11}. It is observed that a significant region under the final drop position (FDP) has a constant pseudo-density i.e. no wettability gradient (NWG) region. Also, a reduction of slope is observed for the region under the initial drop position (IDP). This causes a sharper distribution of wettability in the intermediate region (IR) of the plate, which increases the mean droplet velocity. Here the optimizer deviates from Υ_{qcv}. Note that both IDP and FDP are defined w.r.t Υ_{16}, these regions being shaded in fig. 3b. Optimization on the 8-elements parameterization gives Υ_{12}, where the major change observed is that now, even a fraction of the region under the IDP is a NWG region. Also a bump is observed at the leading edge (LE) of the drop at the IDP, with a peak and valley further along in the IR. Optimization on the 16-elements parameterization gives Υ_{13}, where the major change observed is that the peak is shifted to the LE of the IDP. Also the valley profile is modified in the IR of the plate. Optimization on the 32-elements parameterization converges without any additional major modification. Optimization on the 64-elements parameterization gives Υ_{15}, where the modifications observed were a surge in the peak at the IDP and smoothening of the valley in the IR. The 128-element optimization converges without any additional modification. On the other hand, for an optimization performed directly starting from Υ_{lin} and having a parameterization of 128-elements, the cost function of the resulting profile i.e. Υ_{20} is $\mathcal{J}(\Upsilon_{20}) = 0.009$ l.u./t.s.. Interesting and non obvious features which appear (while using multiscale optimization) are: Firstly, no wettability gradient is required under most of the initial and final location of the droplet to displace the droplet quickly. So, the overall pull-off potential of the WGS is concentrated in the IR having optimal impact on the velocity. Secondly, the optimal (wettability profile) solution is non monotonous, which is counter-intuitive. Although for Υ_{16} the first peak is followed by a deep valley, which ought to cause a local deceleration. This profile is slated to obtain the highest mean droplet velocity. In fact, without this small region defined by the wettability decrease, it would not be possible to reach the performance obtained by the optimizer. Finally, the multiscale feature of the optimization process is very useful, improving the performance by 69 % w.r.t the initial profile i.e. Υ_{lin}. Conversely the performance improvement for optimization only using 128-elements parameterization is 17% w.r.t Υ_{lin}.

B. Sensitivity to the initial wettability profile

The objective of such a study is to check whether or not a single global minimum is reached. For that purpose, different initial wettability profiles have been tested with the multiscale optimizer, namely Υ_{lin} (with $q^{(0)} = 2$), Υ_{qcv} (with $q^{(0)} = 8$) and Υ_{ccv} (with $q^{(0)} = 8$). These simulation have used the smallest plate, with $L = 256$ l.u. and $L/D = 3.2$. Multiscale optimization results are reported in fig. 4. The resulting profiles have the same mean droplet velocity, i.e. $\mathcal{J}(\Upsilon_{16}) = \mathcal{J}(\Upsilon_{21}) = \mathcal{J}(\Upsilon_{22}) \approx 0.0127$ l.u./t.s., but the obtained wettability profiles can be categorized into two groups. The former group is composed of both Υ_{16} and Υ_{21}, where the first peak is observed at the LE of the IDP, followed by a valley in the IR of the plate. Also similar to Υ_{16}, Υ_{21} has no requirement of wettability distribution for significant regions of IDP and FDP in order to propel the droplet to full displacement. On the contrary, for Υ_{22}, a linear wettability slope starting from the beginning of the plate and including the IDP along with most of the IR of the plate is observed. Though the three obtained profiles are identical at the ending part of the plate (from the latter part of the IR to the FDP), taking all into account, it is observed that optimization result is dependent on the shape of the initial wettability profile. This illustrates the dilemma of the non unicity of solution and also the sensitivity of the solution to the initial guess.

Two additional tests are performed to evaluate the cost function for certain non-trivial curves. As a first example, the curve Υ_{23} uses the maximum wettability distribution in the IR along with a fraction of the IDP and the FDP. The obtained corresponding cost function value is much less than for optimized solutions, since $\mathcal{J}(\Upsilon_{23}) = 0.009$ l.u./t.s.. The decrease in performance is attributed to the absence of the peak at the

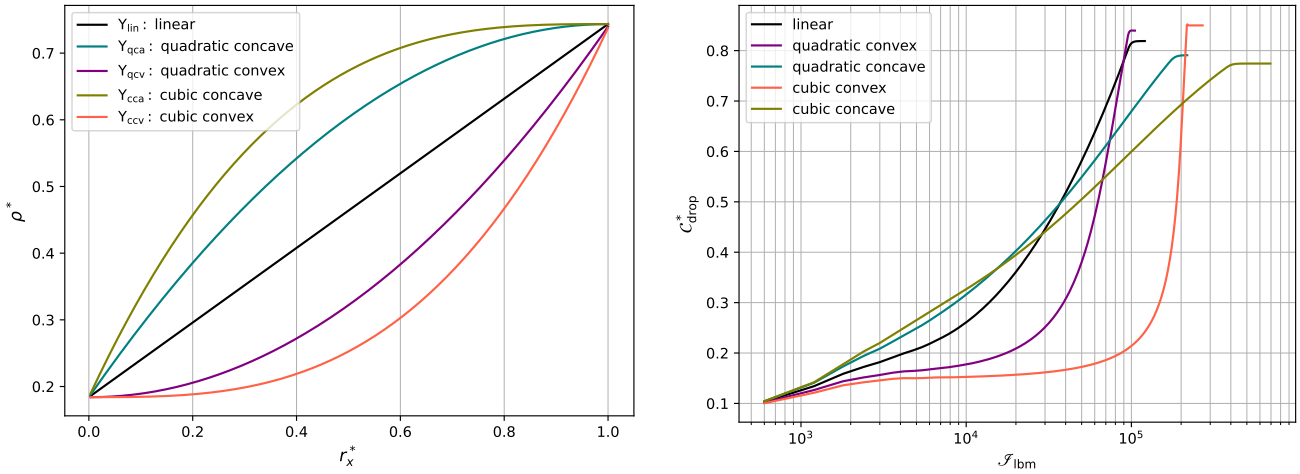

(a) Different initial wettability profiles

(b) Normalized drop center of gravity w.r.t time

Figure 2: Prior to optimization study: performance of wettability profiles for a medium sized plate where $L/D = 6.4$ and $T/T_c = 0.75$

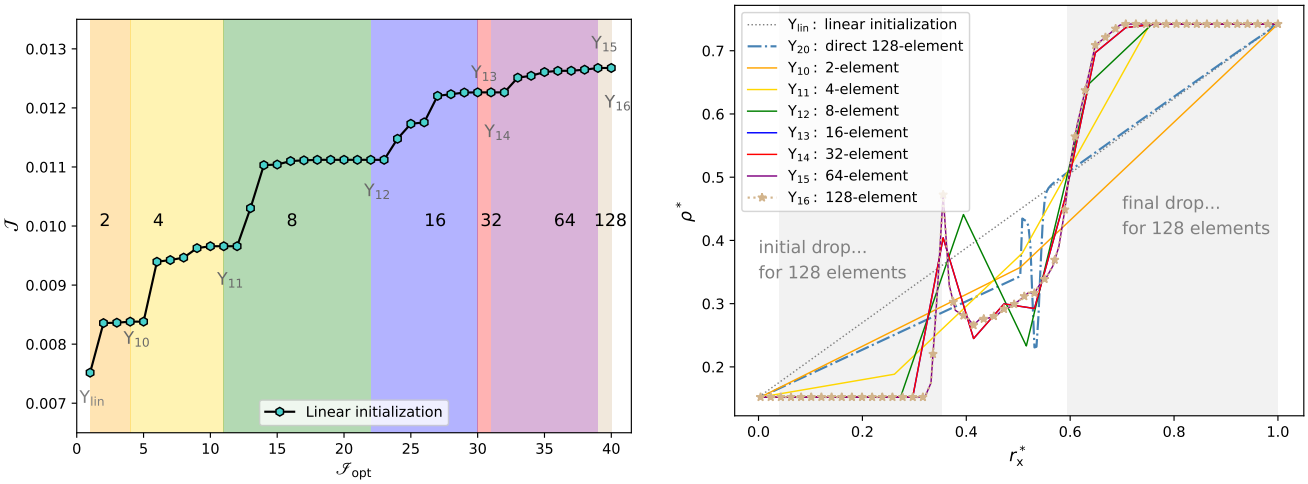

(a) Increase of cost function ($\mathcal{J}$) en-route a multiscale optimization

(b) Intermediate results in a multiscale optimization alongside the direct 128 element optimization

Figure 3: Route/path taken by the multiscale optimization algorithm. The small plate is considered ($L/D = 3.2$) with $T/T_c = 0.75$.

LE of the IDP. As a second example, the curve Υ_{24} is obtained as Υ_{22} is trimmed to a wettability distribution with two linear slopes. The obtained corresponding cost function value is again much less than for optimized solutions, since $\mathcal{J}(\Upsilon_{24}) = 0.008$ l.u./t.s.. Here, the decrease in performance is attributed to the variation of the slope, as compared to Υ_{22} (especially in the latter part of the IR and also the FDP).

Figure 4b depicts the location of the center of gravity with respect to time, transient velocity being simply the local slope of this curve. Analyzing the Υ_{lin} performances, one can recover the classical result: for constant gradient, when the droplet reaches the hydrophilic region, it tends to spread, increasing the contact surface with the solid, and consequently, slows down. Variable wettability gradient profiles, like all the optimization results succeed in preventing this trend, maintaining a higher final velocity

C. Sensitivity to relative droplet and plate sizes

Two series of tests are performed, both dealing with dependency of the optimized solutions to different plate and droplet sizes.

The first series of test considers different droplet diame-

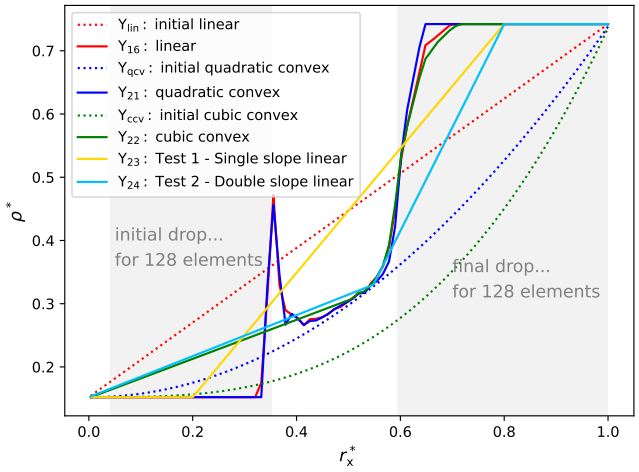

(a) Final and corresponding initialization wettability profiles (along with independent test profiles)

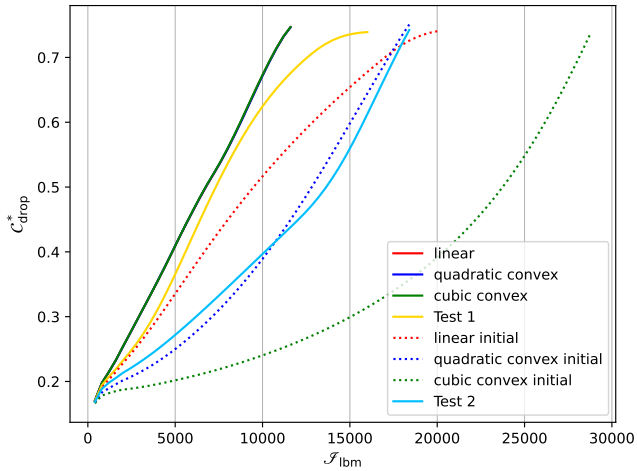

(b) Normalized drop center of gravity(C^*_{drop}) v/s time

Figure 4: Comparing final results for different wettability profile initialization for multiscale optimization for small plate with $L/D = 3.2$ and $T/T_c = 0.75$

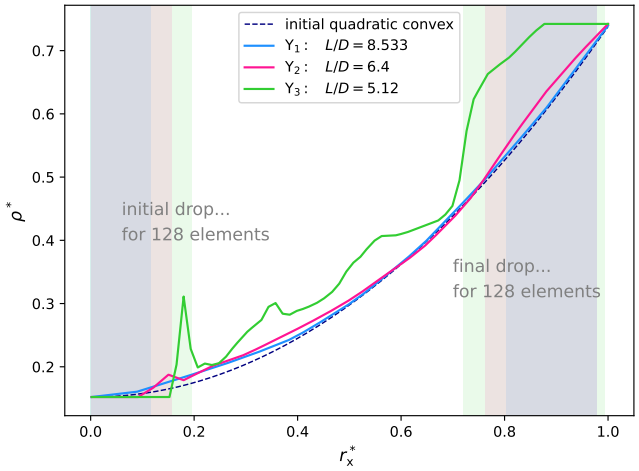

(a) 128 elements result for different droplet diameters ($L/D = 5.12$, $L/D = 6.4$ and $L/D = 8.53$) initialization for multiscale optimization for medium sized plate

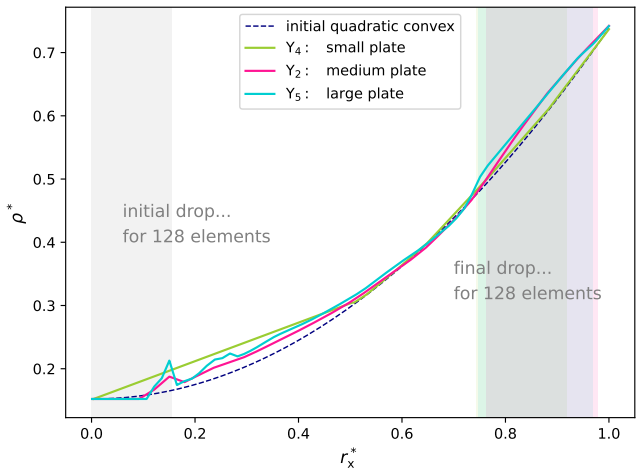

(b) 128 elements result for different plate sizes (small, medium and large) initialization for multiscale optimization with $L/D = 6.4$

Figure 5: Comparing final results for different initialization configuration for multiscale optimization concerning L/D parameter for $T/T_c = 0.75$

ters but with a constant plate size. The medium sized plate has been chosen, and the initial wettability profile is chosen to be the quadratic convex one, Υ_{qcv}. Optimization results are presented in fig. 5a. Optimized profiles Υ_1, Υ_2 and Υ_3 correspond to L/D ratio equal to 8.53, 6.4 and 5.12, respectively. It can be observed from Υ_{21}, Υ_1, Υ_2 and Υ_3 that, as the L/D ratio increases, the obtained profile has lesser bumps and gets progressively smoothened, approaching the initial convex quadratic profile Υ_{qcv}. An explanation for this observation could be that, for lower L/D ratio, a large force – due to a steep bump (large wettability gradient) at the LE of the IDP – is necessary to overcome the inertia of a static droplet. Also, bumps of similar magnitude helps to further maintain the momentum of the droplet at the later stage. The decrease in the volume of liquid drop to be transported causes these bumps to be superfluous.

The second series of test considers different plate sizes but with a constant ratio $L/D = 6.4$. The initial wettability profile is chosen to be the quadratic convex one, Υ_{qcv}. It is here to be pointed out that for a maximum number of elements $q_{\max} = 128$, the minimum optimization element length is $L/q_{\max} = 2$ l.u., 4 l.u. and 8 l.u. for the small, medium and large plates,

respectively. Optimization results are presented in fig. 5b, where profiles Υ_4, Υ_2 and Υ_5 correspond to the small, the medium and the large plate sizes respectively. It is observed that, as the plate size increases, more refined features with defined peaks, dips and valleys are obtained.

D. Applicability of optimization results

The results obtained thus far are for some given prescribed sizes of both a droplet and a table. The question that arises is how a droplet of a given size behaves when being subject to a profile that has been optimized specifically for a another droplet size. Such a cross-check test somehow evaluates the robustness of obtained optimized wettability profiles. This robustness evaluation is of first importance because, though in some controlled applications, e.g. LOC, the droplet sizes are monodisperse (i.e. the variation around the mean droplet size is very small), in other applications, for example in condensation, the droplet sizes are polydisperse (i.e. the variation around the mean droplet size is high). It has thus to be checked whether an optimal profile that has been obtained for a certain droplet size would be appropriate for another droplet size.

Table III gives the computed mean velocity for the three optimal profiles Υ_1, Υ_2 and Υ_3 and for the three L/D ratio. Firstly, it is seen that, for a given L/D ratio, the highest mean velocity is the one obtained with the profile obtained specifically for this L/D ratio, which is not a surprise (these results correspond to cells filled in green in this table). Secondly, for a given L/D ratio, the use of other profiles yields either to lower mean velocity (cells filled in orange in the table) or, worse, to a droplet that never reaches the other end of the plate (cells filled in red in this table). The reasons why the droplet does not reach its destination is either that it is stuck in between two wettability peaks, or that the wettability gradient is too low at its IDP, avoiding any motion right from the beginning. From this result, one conclusion is that, for the specific problem of sequential displacement of droplets with size ranging from $D_{\min}$ to $D_{\max}$ (i.e. assuming no merging of droplets), optimization of the wettability profile must be performed for the smallest one in order to avoid pining of droplets.

Table III also gives the computed mean velocity for the quadratic convex wettability profile. It is seen that the droplet reaches its destination in all cases. Moreover, though the gain of use of optimal profile is not much for large L/D ratio (the gain is 7 % when using Υ_1 instead of using Υ_{lin}), this gain is very high for low L/D ratio (the gain is $\approx$ 44 % when using Υ_3 instead of using Υ_{lin}). Note that, comparing the performance of Υ_{qcv} and Υ_{lin} (from table III) for all of the sampled droplet sizes, it is observed that Υ_{qcv} is consistently better for small displacements.

Table III: Post optimization study: cost function ($\mathcal{J}$) for medium sized plate with different L/D at $T/T_c = 0.75$, (fig. 5a)

Curves	$L/D = 8.53$	$L/D = 6.4$	$L/D = 5.12$
Υ_{qcv}	0.0029 (+0.2% [a])	0.0038 (+0.3%)	0.0045 (+4%)
Υ_1	0.0032 (+7%)	0.0042	0.0048
Υ_2	×[b]	0.0046 (+21%)	0.0051
Υ_3	×	×	0.0062 (+44%)

[a] Performance comparison w.r.t Υ_{lin}.
[b] Droplet does NOT reach the end of plate, hence $\widetilde{C}_{\text{drop}}$ is out of reach.

V. CONCLUSION

Optimization of the wettability gradient surface has been performed in order to increase the mean velocity of a droplet. In order to do so, the pseudo-density (i.e. the control variable) has been tuned; which within the Shan and Chen framework corresponds to locally adjusting the contact angle on the plate (i.e. an ideal surface, without pinning defects or contact angle hysteresis).

Firstly, it has been found that the multiscale approach is necessary in order to converge to some optimal robust solutions.

Secondly, for large expected displacements, the proposed quadratic convex wettability profile appears to be a good candidate. On the other hand, for small expected displacements, optimizing the wettability profile is of prime importance as it allows an increase of up to 69 % of the mean velocity when compared to the use of a classical linear wettability profile.

Thirdly, optimization results exhibit some non trivial features. At first, no wettability gradient is needed under most of the initial and the final droplet locations, allowing to focus the potential of the wettability tuning on a smaller area, enhancing its effect. Another interesting feature is the existence of some non monotonous optimal profiles. Indeed, starting with a steep initial profile allows to quickly overcome the inertia, this being followed by an unexpected decrease of the wettability which does not result in a pinning droplet.

Conclusions of this numerical work will be vetted in the future by experimental means, having in mind that many industrial applications could benefit from this, for example lab-on-a-chip.

Acknowledgments

The authors thank Le Centre de calcul intensif des Pays de la Loire (CCIPL), for access to its Nvidia Tesla T4 GPUs. Also the authors declare no conflict of interest.

Appendix A: Interpolation equations for Υ as used in fig. 2

Using the notations $\rho_{\text{w}}^{\max} = \rho^+$ at r_x^+, $\rho_{\text{w}}^{\min} = \rho^-$ at r_x^-, $\Delta\rho = \rho^+ - \rho^-$ and $\Delta r_x = r_x^+ - r_x^-$ it is possible to write the interpolation equations as:

- Linear evolution (passes by both end points):

$$\rho_{\text{w}}^1(r_x) = \rho^+ - \frac{\Delta\rho}{\Delta r_x}(r_x^+ - r_x)$$

- Quadratic convex (passes by both end points plus null derivative on r_x^- – no linear term):

$$\rho_w^{2,\cup}(r_x) = \rho^- + \frac{\Delta\rho}{\Delta r_x^2}(r_x^- - r_x)^2$$

- Quadratic concave (passes by both end points plus null derivative on r_x^+ – no linear term):

$$\rho_w^{2,\cap}(r_x) = \rho^+ - \frac{\Delta\rho}{\Delta r_x^2}(r_x^+ - r_x)^2$$

- Cubic convex (passes by both end points plus null derivative on r_x^- – no linear and quadratic terms):

$$\rho_w^{3,\cup}(r_x) = \rho^- + \frac{\Delta\rho}{\Delta r_x^3}(r_x^- - r_x)^3$$

- Quadratic concave (passes by both end points plus null derivative on r_x^+ – no linear and quadratic terms):

$$\rho_w^{3,\cap}(r_x) = \rho^+ - \frac{\Delta\rho}{\Delta r_x^3}(r_x^+ - r_x)^3$$

Appendix B: Validation for SCMP pseudopotential model

Generally, as a droplet is propelled on a WGS, its velocity ($\mathbf{v}_{drop}$) varies in accordance with the local gradient of wettability (under the belly of the droplet). For wettability gradient of low intensity, $\mathbf{v}_{drop}$ approaches an asymptotic value, i.e. a constant droplet velocity is observed for significant duration of the droplet journey. This is also known as migration velocity ($\mathbf{v}_{mig}$) of the droplet and is expressed as[16,28]:

$$\mathbf{v}_{mig} = \alpha_v \frac{\sigma h_0}{\nu_{liq}\rho_{liq}} \left(\frac{\mathrm{d}\cos(\theta_{stat})}{\mathrm{d}r_x}\right) \tag{B1}$$

where h_0 is the initial height of the droplet and α_v is the constant of proportionality. It is observed[16] that the numerically obtained migration velocity (V_{mig}) is linearly proportional to the intensity of the wettability gradient. For a simulation on the small plate, the droplet size is such that $L/D = 4.51$, while the surface tension of the liquid is $\sigma = 0.003$. The Bond number of the simulation is Bo = 0.018294 with the corresponding density ratio being $\rho_{liq}/\rho_{vap} = 7.35$ at temperature $T/T_c = 0.875$, the forward problem successfully reproduces the linearity for hydrophilic wettability distributions, as shown in fig. 6 (all values in fig. 6 are mentioned in LBM units).

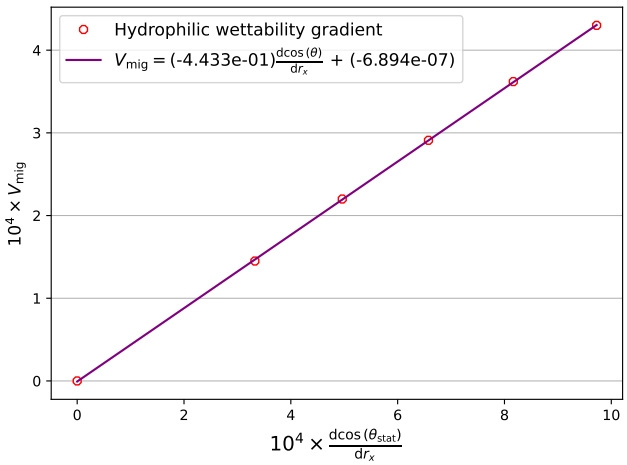

Figure 6: Correlation between asymptotic velocity i.e. migration velocity (V_{mig}) and intensity of the wettability gradient on a WGS (at $T/T_c = 0.875$).

REFERENCES

[1] S. Feng, P. Zhu, H. Zheng, H. Zhan, C. Chen, J. Li, L. Wang, X. Yao, Y. Liu, and Z. Wang, "Three-dimensional capillary ratchet-induced liquid directional steering," Science **373**, 1344–1348 (2021), publisher: American Association for the Advancement of Science.

[2] F. Shan, Z. Chai, B. Shi, J. Xiao, and C. Wang, "Directional transport of a droplet on biomimetic ratchet structure," Physics of Fluids **35**, 113314 (2023).

[3] V. Baghel and M. Ranjan, "Numerical estimation of droplet motion on linear wettability gradient surface in microgravity environment," Materials Today Communications **32**, 103916 (2022).

[4] Y. Sui, "Moving towards the cold region or the hot region? Thermocapillary migration of a droplet attached on a horizontal substrate," Physics of Fluids **26**, 092102 (2014).

[5] C. Marangoni, "Sull'espansione delle goccie d'un liquido galleggianti sulla superfice di altro liquido," (1865).

[6] P. Brunet, J. Eggers, and R. D. Deegan, "Vibration-Induced Climbing of Drops," Physical Review Letters **99**, 144501 (2007), publisher: American Physical Society.

[7] R. J. Petrie, T. Bailey, C. B. Gorman, and J. Genzer, "Fast Directed Motion of "Fakir" Droplets," Langmuir **20**, 9893–9896 (2004).

[8] G. Fang, W. Li, X. Wang, and G. Qiao, "Droplet Motion on Designed Microtextured Superhydrophobic Surfaces with Tunable Wettability," Langmuir **24**, 11651–11660 (2008).

[9] L. Jin and Y. Wang, "Control the droplet motion by using chemically stripe-patterned surfaces," Chemical Physics **532**, 110678 (2020).

[10] M. S. Maria, P. E. Rakesh, T. S. Chandra, and A. K. Sen, "Capillary flow-driven microfluidic device with wettability gradient and sedimentation effects for blood plasma separation," Scientific Reports **7**, 43457 (2017), number: 1 Publisher: Nature Publishing Group.

[11] D. Attinger, C. Frankiewicz, A. R. Betz, T. M. Schutzius, R. Ganguly, A. Das, C.-J. Kim, and C. M. Megaridis, "Surface engineering for phase change heat transfer: a review," MRS Energy & Sustainability **1**, 4 (2014), number: 1.

[12] M. Alwazzan, K. Egab, B. Peng, J. Khan, and C. Li, "Condensation on hybrid-patterned copper tubes (i): Characterization of condensation heat transfer," International Journal of Heat and Mass Transfer **112**, 991–1004 (2017).

[13] S. Tang, Q. Li, Y. Yu, and Y. Qiu, "Enhancing dropwise condensation on downward-facing surfaces through the synergistic effects of surface structure and mixed wettability," Physics of Fluids **33**, 083301 (2021), number: 8.

[14] B. S. Yilbas, G. Hassan, A. Al-Sharafi, H. Ali, N. Al-Aqeeli, and A. Al-Sarkhi, "Water Droplet Dynamics on a Hydrophobic Surface in Relation to the Self-Cleaning of Environmental Dust," Scientific Reports **8**, 2984 (2018).

[15] M. Yakubu, B. S. Yilbas, A. A. Abubakr, and H. Al-Qahtani, "Droplet Rolling and Spinning in V-Shaped Hydrophobic Surfaces for Environmental Dust Mitigation," Molecules **25**, 3039 (2020).

[16] F. Brochard, "Motions of droplets on solid surfaces induced by chemical or

thermal gradients," Langmuir **5**, 432–438 (1989).
[17] H. P. Greenspan, "On the motion of a small viscous droplet that wets a surface," Journal of Fluid Mechanics **84**, 125–143 (1978).
[18] M. K. Chaudhury and G. M. Whitesides, "How to Make Water Run Uphill," Science **256**, 1539–1541 (1992), publisher: American Association for the Advancement of Science.
[19] R. S. Subramanian, N. Moumen, and J. B. McLaughlin, "Motion of a Drop on a Solid Surface Due to a Wettability Gradient," Langmuir **21**, 11844–11849 (2005), publisher: American Chemical Society.
[20] L. M. Pismen and U. Thiele, "Asymptotic theory for a moving droplet driven by a wettability gradient," Physics of Fluids **18**, 042104 (2006).
[21] J. Huang, C. Shu, and Y. Chew, "Numerical investigation of transporting droplets by spatiotemporally controlling substrate wettability," Journal of Colloid and Interface Science **328**, 124–133 (2008).
[22] U. Thiele, K. John, and M. Bär, "Dynamical Model for Chemically Driven Running Droplets," Physical Review Letters **93**, 027802 (2004).
[23] I. U. Chowdhury, P. S. Mahapatra, and A. K. Sen, "Shape evolution of drops on surfaces of different wettability gradients," Chemical Engineering Science **229**, 116136 (2021).
[24] Q. Chang and J. I. D. Alexander, "Analysis of single droplet dynamics on striped surface domains using a lattice Boltzmann method," Microfluidics and Nanofluidics **2**, 309–326 (2006).
[25] A. Onuki, "Dynamic van der Waals theory," Physical Review E **75**, 036304 (2007).
[26] Q. Kang, D. Zhang, and S. Chen, "Displacement of a two-dimensional immiscible droplet in a channel," Physics of Fluids **14**, 3203–3214 (2002).
[27] T. Krüger, H. Kusumaatmaja, A. Kuzmin, O. Shardt, G. Silva, and V. E., M., *The Lattice Boltzmann Method: Principles and Practice* (Springer International Publishing, 2017).
[28] X. Xu and T. Qian, "Droplet motion in one-component fluids on solid substrates with wettability gradients," Physical Review E **85**, 051601 (2012).
[29] A. Fikl and D. J. Bodony, "Adjoint-based interfacial control of viscous drops," Journal of Fluid Mechanics **911**, A39 (2021).
[30] A. Fikl and D. J. Bodony, "Adjoint-based control of three dimensional stokes droplets," Journal of Computational Physics **494**, 112532 (2023).
[31] B. Yin, S. Xu, S. Yang, and F. Dong, "Shape optimization of a microhole surface for control of droplet wettability via the lattice boltzmann method and response surface methodology," Langmuir **37** (2021), 10.1021/acs.langmuir.0c03596.
[32] E. W. Weisstein, "Brachistochrone Problem," Publisher: Wolfram Research, Inc.
[33] M. Sukop and D. Thorne, *Lattice Boltzmann Modeling-An Introduction for Geoscientists and Engineers* (Springer-Verlag Berlin Heidelberg, 2006).
[34] H. Huang, M. Krafczyk, and X. Lu, "Forcing term in single-phase and shan-chen-type multiphase lattice boltzmann models," Physical review. E, Statistical, nonlinear, and soft matter physics **84**, 046710 (2011).
[35] X. Shan and H. Chen, "Simulation of nonideal gases and liquid-gas phase transitions by the lattice boltzmann equation," Phys. Rev. E **49**, 2941–2948 (1994).
[36] "Generalized lattice-boltzmann equations," in *Rarefied Gas Dynamics: Theory and Simulations*, pp. 450–458, https://arc.aiaa.org/doi/pdf/10.2514/5.9781600866319.0450.0458.
[37] M. Bouzidi, D. d'Humières, P. Lallemand, and L.-S. Luo, "Lattice boltzmann equation on a two-dimensional rectangular grid," Journal of Computational Physics **172**, 704–717 (2001).
[38] A. Kupershtokh, D. Medvedev, and D. Karpov, "On equations of state in a lattice boltzmann method," Computers & Mathematics with Applications **58**, 965 – 974 (2009), mesoscopic Methods in Engineering and Science.
[39] P. Yuan and L. Schaefer, "Equations of state in a lattice boltzmann model," Physics of Fluids **18**, 042101 (2006), https://doi.org/10.1063/1.2187070.
[40] H. Huang and M. Krafczyk, "Comment on "lattice boltzmann method for simulations of liquid-vapor thermal flows"," Physical review. E, Statistical, nonlinear, and soft matter physics **84**, 038701; discussion 038702 (2011).
[41] J. Nocedal and J. Wright, Stephen, *Numerical Optimization* (Springer New York, NY, 2006).
[42] G. Chavent, *Nonlinear least squares for inverse problems: theoretical foundations and step-by-step guide for applications* (Springer Science & Business Media, 2010).